JOURNAL OF COMPUTATIONAL PHYSICS 24, 158–185 (1977)

A Numerical Model for Resistive Magnetohydrodynamic Instabilities*

JAMES A. DIBIASE AND JOHN KILLEEN

Lawrence Livermore Laboratory, Livermore, California 94550, and
Department of Applied Science, University of California, Davis/Livermore, California 94550

Received November 2, 1976; revised December 16, 1976

A hydromagnetic model has been developed to study resistive instabilities in cylindrical geometry, and the model is applied to study specific diffuse pinch configurations. The MHD equations include the effects of compressibility, finite resistivity, viscosity, and thermal conductivity. The plasma equilibrium configuration is assumed known and is specified by $B_{\theta 0}(r)$, $B_{z0}(r)$, $\eta_0(r)$, $\rho_0(r)$, $T_0(r)$ and these functions can be chosen to describe a particular experiment. Perturbations of the form $f_1(r, t) \exp[i(m\theta + k_z z)]$ are used for all plasma and field variables, and the resulting linear partial differential equations are solved numerically as an initial value problem using an implicit difference scheme. A set of seven equations for B_{r1}, $B_{\theta 1}$, T_1, v_{r1}, $v_{\theta 1}$, v_{z1}, ρ_1 is obtained and the calculation is started by specifying an initial perturbation. For a particular problem, the parameters m, k_z, and $S = \tau_R/\tau_H$, the ratio of resistive diffusion time to hydromagnetic transit time must be given, and for certain choices an exponential growth occurs and the growth rate $p(m, k_z, S)$ is calculated.

1. INTRODUCTION

In order to achieve the high densities and temperatures required for a successful thermonuclear reactor, a plasma must be confined by a magnetic field for a sufficiently long time. In the attempts to achieve this confinement, the problem of stability has emerged as one of the most important. A plasma confined by a magnetic field is potentially able to break out of the confinement system by a large variety of instabilities, and a number of field configurations have been proposed which could confine a hot plasma in equilibrium, if such configurations were stable.

The most dangerous type of instabilities are the magnetohydrodynamic (MHD) or hydromagnetic instabilities in which the plasma is assumed to behave as a conducting fluid and the instabilities involve displacement of macroscopic portions of the plasma. It is a particular MHD instability, the resistive instability, which is considered in this paper.

One of the earliest plasma confinement schemes tested was that of the pinch effect in which an axial current in a cylindrical plasma produces an azimuthal field that

* Work performed under the auspices of the U.S. Energy Research and Development Administration. Contract Number W-7405-ENG-48.

ISSN 0021-9991

constricts or pinches the plasma. It has been found both theoretically and experimentally that such pinch configurations are unstable to MHD type instabilities, and the four lowest order distortions are shown schematically in Fig. 1. The $m = 1$ kink instability is usually the most dangerous since it allows the plasma to break through the confining magnetic field to reach the walls.

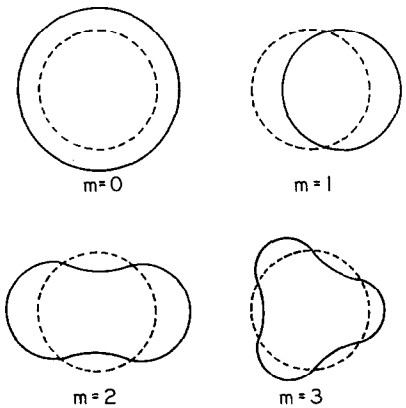

FIG. 1. The four lowest-order distortions for a cylindrical plasma. The dotted lines represent the equilibrium cross section.

The pinch can be made more stable if a magnetic field parallel to the axis is trapped within the cylinder and if there is an azimuthal external field generated by a current at the surface of the plasma column. For this configuration, the sausage ($m = 0$) and kink ($m = 1$) instabilities bend and compress the field lines, bringing into play forces which oppose the growth of the instability. Unfortunately, it has not proven possible to stabilize the pinch completely, since in reality the current flows in a layer of finite thickness and a localized instability can develop. In the present analysis, a pinch configuration is established in which the plasma currents are assumed to be diffuse, i.e., the axial and azimuthal currents are not restricted to a thin plasma sheath but are uniformly distributed throughout the plasma. The plasma is assumed to completely fill an infinitely long plasma cylinder.

Resistivity can destroy the stabilization achieved by the shearing of the lines of force. In the case of a magnetic field which has shear or which changes direction as illustrated in Fig. 2c, the magnetic energy can be reduced by allowing the fields to mix and annihilate. This is prevented by a perfectly conducting plasma. However, for finite conductivity an instability can develop in which the magnetic lines of force, as shown in Fig. 2a, are torn into loops or rings, as shown in Fig. 2d. This type of resistive instability is known as a resistive tearing mode [1].

There are three types of resistive modes: (1) the rippling mode, which is driven by a gradient in the resistivity and is usually not important at high beta where large temperature gradients are unlikely; (2) the gravitational mode (g-mode) which is the resistive equivalent of the interchange instability and is important in sheared systems;

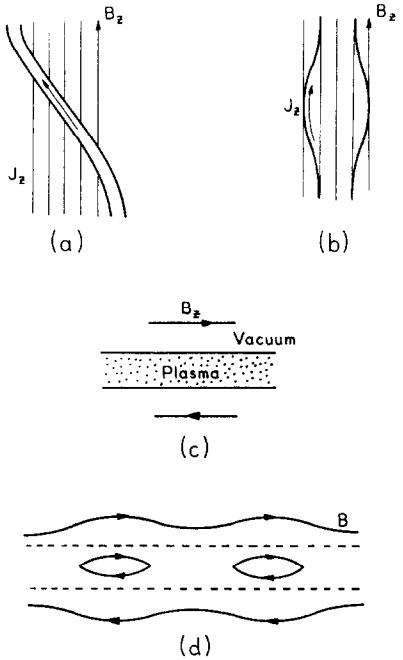

FIG. 2. Resistive instabilities: (a) stabilized pinch with kink in J ($m = 1$); (b) stabilized pinch with sausage in J ($m = 0$); (c) reversed field layer; (d) resistive tearing instability of reversed field layer.

and (3) the tearing mode, which is the resistive equivalent of the kink mode and involves displacement of the whole plasma. The last two modes are important at high beta, and both are found using resistive MHD theory.

The tearing mode differs from the other two modes in that it is typically a long-wave rather than a short-wave mode relative to the dimension of the current layer, and consequently it is expected that it would be stabilized by conducting walls. The driving force is due to the structure of the magnetic field outside the region of decoupled flow, i.e., the tendency of a sheet current to break up into a set of parallel pinches. The modes grow on a time scale intermediate between the resistive diffusion time $\tau_R = 4\pi a^2/\eta c^2$ and the hydromagnetic transit time $\tau_H = a(4\pi\rho)^{1/2} B^{-1}$ where a is a characteristic dimension of the plasma layer, η is the resistivity, ρ is the mass density of the plasma, B is the magnetic field, and c is the speed of light. For theory to apply, it is required that $S = \tau_R/\tau_H \gg 1$.

The basic paper on resistive MHD instabilities is that by FKR [1] who analytically treat all of the possible linear resistive instabilities of a plane plasma sheet in a sheared magnetic field configuration, and describe in detail the driving forces of the instabilities. Similar analyses have been done in cylindrical geometry by Coppi *et al.* [2] who examined resistive instabilities for a diffuse linear pinch. In addition, Coppi *et al.* [2] considered the effects of viscosity and thermal conductivity and found that viscosity can have a stabilizing effect on resistive modes.

Due to the many possible equilibrium configurations and the many approximations necessary to make the problem analytically tractable, it is usually not possible to analytically describe the general parameter dependence of the growth rates of the resistive instabilities. Also, the analytic tratments are usually done in the limits of high and low S. In order to supplement the analyses for intermediate values of S and to be able to obtain results for specific and wide choices of equilibrium magnetic fields and boundary conditions, numerical models have been developed to study these resistive instabilities.

The numerical models are based on the linearized equations which assume an arbitrary time dependence, i.e., the hydromagnetic equations are Fourier analyzed in space but not in time, and the problem becomes an initial-value problem for the perturbed quantities. Also, two regions are not used, instead the same resistive equations are assumed to hold throughout the plasma. The parameters, initial conditions, boundary conditions, and type of modes to be examined can all be varied.

Based on the incompressible hydromagnetic equations, a time-dependent, resistive instability computational model for both Cartesian and cylindrical geometry was developed by Killeen [3] and has been applied to the Triax experiment, hardcore pinch configurations, the thetatron, and to a force-free Bessel function model, [4] all of which were tearing mode calculations. The general computational model used included resistive and gravitational effects due to convection.

In this paper, a new cylindrical model is developed; a general model which includes the effects of compressibility, finite resistvity, viscosity, and thermal conductivity. In Section 2 the specific equations used in the model are presented, and in Section 3 the finite-difference equations are presented and the method of solution is described. In Section 4 the computational model is applied to different types of equilibrium magnetic field configurations. The equilibrium configurations are tested for resistive tearing instabilities in the parameter space about which $\bar{k} \cdot \bar{B} = 0$. Growth rates are calculated for various (m, k_z) modes and the results are presented in the form of stability diagrams. Additional parametric studies are also performed to determine the specific dependence of the growth rates on the position of outer conducting wall R_w, the axial wave number k_z, and the magnetic Reynolds number S.

2. Mathematical Model

We describe the plasma by the equations of magnetohydrodynamics for a single fluid. Thermal conductivity, electrical resistivity, and viscosity are included and are assumed to be scalar functions. The continuity equation is

$$(\partial\rho/\partial t) + \nabla \cdot (\rho \mathbf{v}) = 0 \tag{1}$$

where ρ and $\mathbf{v}$ are fluid density and velocity. The equation of motion is

$$\rho((\partial \mathbf{v}/\partial t) + \mathbf{v} \cdot \nabla \mathbf{v}) = (1/c)(\mathbf{j} \times \mathbf{B}) - \nabla p + \rho\nu[\nabla^2 \mathbf{v} + \tfrac{1}{3}\nabla(\nabla \cdot \mathbf{v})] \tag{2}$$

where p is the pressure, $\mathbf{j}$ is the current density, $\mathbf{B}$ is the magnetic field, ν is the coefficient of kinematic viscosity. The energy equation is

$$\rho((\partial T/\partial t) + \mathbf{v} \cdot \nabla T) = -(\gamma - 1)\,\rho T(\nabla \cdot \mathbf{v}) + K\nabla^2 T + (\gamma - 1)\,\eta\,|\,\mathbf{j}\,|^2 + (\gamma - 1)\,\rho\nu[|\,\nabla \times \mathbf{v}\,|^2 + \tfrac{4}{3}(\nabla \cdot \mathbf{v})^2] \tag{3}$$

where T is the plasma temperature, K is the thermal conductivity, γ is the gas constant, η is the resistivity. The equation of state is $p = \rho T$ and the Ohm's law is given by

$$\mathbf{E} + (1/c)(\mathbf{v} \times \mathbf{B}) = \eta\mathbf{j} \tag{4}$$

where $\mathbf{E}$ is the electric field. To complete the system we take the following Maxwell equations

$$\nabla \times \mathbf{E} = -(1/c)(\partial\mathbf{B}/\partial t), \tag{5}$$

$$\nabla \times \mathbf{B} = (4\pi/c)\,\mathbf{j}, \tag{6}$$

$$\nabla \cdot \mathbf{B} = 0. \tag{7}$$

We can combine Eqs. (4), (5), and (6) to give

$$\partial\mathbf{B}/\partial t = \nabla \times (\mathbf{v} \times \mathbf{B}) - (c^2/4\pi)\,\nabla \times (\eta\nabla \times \mathbf{B}). \tag{8}$$

The plasma equilibrium is specified by $\mathbf{v}_0 = 0$ and given functions $\mathbf{B}_0$, T_0, and ρ_0 which satisfy the zero-order equations

$$\frac{1}{4\pi}(\nabla \times \mathbf{B}_0) \times \mathbf{B}_0 - \nabla(\rho_0 T_0) = 0, \tag{9}$$

$$K\nabla^2 T_0 + (\gamma - 1)\,\eta_0 \left(\frac{c}{4\pi}\right)^2 (\nabla \times \mathbf{B}_0) \cdot (\nabla \times \mathbf{B}_0) = 0, \tag{10}$$

$$\nabla \times (\eta_0 \nabla \times \mathbf{B}_0) = 0. \tag{11}$$

We denote perturbed quantities by the subscript 1. The equations for the first-order variables are linearized and are given by

$$(\partial\rho_1/\partial t) + \nabla \cdot (\rho_0 \mathbf{v}_1) = 0, \tag{12}$$

$$\rho_0 \frac{\partial \mathbf{v}_1}{\partial t} = \frac{1}{4\pi}[(\mathbf{B}_0 \cdot \nabla)\,\mathbf{B}_1 + (\mathbf{B}_1 \cdot \nabla)\,\mathbf{B}_0 - \nabla(\mathbf{B}_0 \cdot \mathbf{B}_1)] - \nabla(\rho_0 T_1) - \nabla(\rho_1 T_0) + \rho_0\nu[\tfrac{1}{3}\nabla(\nabla \cdot \mathbf{v}_1) + \nabla^2\mathbf{v}_1], \tag{13}$$

$$\rho_0 \frac{\partial T_1}{\partial t} = -\rho_0(\mathbf{v}_1 \cdot \nabla)\,T_0 - (\gamma - 1)\,\rho_0 T_0(\nabla \cdot \mathbf{v}_1) + K\nabla^2 T_1 + (\gamma - 1)\left(\frac{c}{4\pi}\right)^2 [2\eta_0(\nabla \times \mathbf{B}_0) \cdot (\nabla \times \mathbf{B}_1) + \eta_1(\nabla \times \mathbf{B}_0) \cdot (\nabla \times \mathbf{B}_0)], \tag{14}$$

$$\frac{\partial \mathbf{B}_1}{\partial t} = \nabla \times (\mathbf{v}_1 \times \mathbf{B}_0) - \frac{c^2}{4\pi}\nabla \times [\eta_0 \nabla \times \mathbf{B}_1 + \eta_1 \nabla \times \mathbf{B}_0]. \tag{15}$$

We solve the system of equations (12)–(15) in cylindrical coordinates r, θ, and z. The plasma equilibrium configuration is given by

$$\mathbf{B}_0 = \hat{\theta} B_{\theta 0}(r) + \hat{Z} B_{z0}(r),$$
$$\mathbf{v}_0 = 0, \qquad T_0 = T_0(r), \qquad \rho_0 = \rho_0(r), \qquad \eta_0 = \eta_0(r).$$

These functions are chosen to describe a particular experiment; in a toroidal device $B_{\theta 0}$ is called the poloidal field, and B_{z0} is called the toroidal field.

We assume perturbations of the form

$$f_1(r, t)\, e^{i(m\theta + k_z z)}.$$

From Eqs. (12)–(15) we obtain seven equations for $B_{r1}(r, t)$, $B_{\theta 1}(r, t)$, $v_{r1}(r, t)$, $v_{\theta 1}(r, t,)$ $v_{z1}(r, t)$, $T(r, t)$, and $\rho_1(r, t)$. The character of these partial differential equations and their associated boundary conditions require an implicit finite-difference scheme such as that used to solve coupled diffusion equations.

In order to solve the systems of equations on the domain $0 \leqslant r \leqslant R_W$, where R_W is the radius of the outer conducting wall, boundary conditions must be specified at both $r = 0$ and $r = R_W$. For a numerical solution, a boundedness condition at $r = 0$ is not sufficient, therefore the following symmetry conditions are used at $r = 0$ for all t

$\underline{m = 0}$

$$B_{r1} = B_{\theta 1} = v_{r1} = v_{\theta 1} = 0, \qquad \frac{\partial v_{z1}}{\partial r} = \frac{\partial T_1}{\partial r} = \frac{\partial \rho_1}{\partial r} = 0. \tag{16}$$

$\underline{m = 1}$

$$\frac{\partial B_{r1}}{\partial r} = \frac{\partial B_{\theta 1}}{\partial r} = \frac{\partial v_{r1}}{\partial r} = \frac{\partial v_{\theta 1}}{\partial r} = 0, \qquad v_{z1} = T_1 = \rho_1 = 0. \tag{17}$$

$\underline{m \geqslant 2}$

$$B_{r1} = B_{\theta 1} = T_1 = v_{r1} = v_{\theta 1} = v_{z1} = \rho_1 = 0. \tag{18}$$

Using the premise that the perturbed radial current vanishes at the outer wall R_W, Robinson [5] has used the infinite conductivity MHD theory to derive the following set of boundary conditions at R_W

$$B_{r1}(R_W, t) = v_{r1}(R_W, t) = T_1(R_W, t) = \rho_1(R_W, t) = 0, \tag{19}$$

$$B_{\theta 1}(R_W, t) = \frac{imR_W}{m^2 + k_z^2 R_W^2} \frac{\partial B_{r1}}{\partial r}\bigg|_{r=R_W}, \tag{20}$$

$$v_{\theta 1}(R_W, t) = \frac{imR_W}{m^2 + k_z^2 R_W^2} \frac{\partial v_{r1}}{\partial r}\bigg|_{r=R_W}, \tag{21}$$

$$v_{z1}(R_W, t) = \frac{ik_z R_W^2}{m^2 + k_z^2 R_W^2} \frac{\partial v_{r1}}{\partial r}\bigg|_{r=R_W}. \tag{22}$$

These conditions are valid provided $\bar{k} \cdot \bar{B} \neq 0$ at the wall and that the density ρ_0, temperature T_0, and pressure p_0 tend to zero as $r \to R_W$. Note that the systems of equations are solved throughout the domain $0 \leqslant r \leqslant R_W$, i.e., there is not a plasma region surrounded by a vacuum region nor is there a plasma region of finite conductivity surrounded by a region of infinite conductivity.

3. Finite-Difference Equations and Method of Solution

3.1. *Dimensionless Equations*

It is convenient to put the systems of hydromagnetic equations into dimensionless form. The two relevant times for the problem are the decay time of the equilibrium magnetic field or the resistive diffusion time

$$\tau_R = 4\pi a^2/c^2\langle\eta\rangle, \tag{23}$$

and the hydromagnetic (or Alfvén-wave) transit time

$$\tau_H = a(4\pi\langle\rho\rangle)^{1/2}/B, \tag{24}$$

where a is a characteristic length which is usually a measure of the thickness of the current layer, and B, $\langle\eta\rangle$, and $\langle\rho\rangle$ are characteristic values for the magnetic field, resistivity, and mass density, respectively. The two dimensionless independent variables are defined as

$$\mu = r/a, \qquad \tau = t/\tau_R. \tag{25}$$

If R is the value of r such that

$$\bar{k} \cdot \bar{B} = (m/r)\, B_{\theta 0} + k_z B_{z0} = 0, \tag{26}$$

then R is the radius about which the instability will develop if the equilibrium configuration is resistively unstable for the particular mode specified by the pair of mode numbers m and k_z [1, 4]. In the cylindrical geometry used here, these two mode numbers are specified independently, while in the planar sheet pinch model [1] only one number is required to describe a particular mode.

The dimensionless dependent variables are defined as

$$\begin{aligned}
&\psi = \frac{B_{r1}}{B} && \phi = i\frac{B_{\theta 1}}{B} && \Upsilon = \frac{iT_1}{\langle T\rangle} \\
&W = -ik\tau_R v_{r1} && U = k\tau_R v_{\theta 1} && V = k\tau_R v_{z1} \\
&\mathscr{R} = \frac{i\rho_1}{\langle\rho\rangle} && \delta = -i\frac{\eta_1}{\langle\eta\rangle} && P = \frac{ip_1}{\langle\rho\rangle\langle T\rangle}
\end{aligned} \tag{27}$$

where $k = (m^2/R^2 + k_z^2)^{1/2}$ and $\langle T \rangle$ is a characteristic value for the (normalized) temperature in units of energy/mass. The following parameters are also required:

$$\alpha = ka, \tag{28}$$

$$\kappa_z = k_z a, \tag{29}$$

$$S \equiv \frac{\tau_R}{\tau_H} = \frac{(4\pi)^{1/2}\, aB}{c^2 \langle \eta \rangle \langle \rho \rangle^{1/2}}, \tag{30}$$

$$\Gamma \equiv \frac{4\pi\nu}{c^2 \langle \eta \rangle} = \frac{\tau_R \nu}{a^2}, \tag{31}$$

$$\Lambda \equiv \frac{4\pi K}{c^2 \langle \eta \rangle \langle \rho \rangle} = \frac{\tau_R K}{a^2 \langle \rho \rangle}, \tag{32}$$

$$\beta = \frac{8\pi \langle \rho \rangle \langle T \rangle}{B^2}, \tag{33}$$

where S is the magnetic Reynolds number, Γ is a dimensionless viscosity, Λ is a dimensionless thermal conductivity, and β is the plasma beta which is the usual ratio of the fluid pressure to the pressure in the magnetic field.

The following functions are given by the equilibrium configuration:

$$\begin{aligned}
&H = \frac{B_{\theta 0}}{B} \qquad M = \frac{B_{z0}}{B}, \\
&F = \frac{1}{kB}\left(\frac{m}{r} B_{\theta 0} + k_z B_{z0}\right) = \frac{1}{\alpha}\left(\frac{m}{\mu} H + \kappa_z M\right), \\
&F' = \frac{dF}{d\mu} \qquad F'' = \frac{d^2F}{d\mu^2}, \\
&M' = \frac{dM}{d\mu} \qquad M'' = \frac{d^2M}{d\mu^2}, \\
&H' = \frac{dH}{d\mu} \qquad H'' = \frac{d^2H}{d\mu^2} \qquad H''' = \frac{d^3H}{d\mu^3}, \\
&N = \frac{1}{\mu}\frac{\partial}{\partial \mu}(\mu H) \qquad N' = \frac{dN}{d\mu} \qquad N'' = \frac{d^2N}{d\mu^2}, \\
&\tilde{\rho} = \frac{\rho_0}{\langle \rho \rangle} \qquad \tilde{T} = \frac{T_0}{\langle T \rangle} \qquad \tilde{\eta} = \frac{\eta_0}{\langle \eta \rangle}, \\
&\tilde{\rho}' = \frac{d\rho}{d\mu} \qquad \tilde{T}' = \frac{dT}{d\mu} \qquad \tilde{\eta}' = \frac{d\eta}{d\mu} \\
&\qquad\qquad \tilde{p} = \frac{p_0}{\langle \rho \rangle \langle T \rangle}.
\end{aligned} \tag{34}$$

Defining the operator

$$L \equiv \frac{\partial^2}{\partial \mu^2} + \frac{1}{\mu}\frac{\partial}{\partial \mu} - \left(\frac{m^2 + 1}{\mu^2} + \kappa_z^2\right), \tag{35}$$

the systems of dimensionless equations can be put into a more compact form.

TABLE 3.1

Component Equations

(1) $$\frac{\partial \psi}{\partial \tau} = -FW + \tilde{\eta}\left(L\psi - \frac{2m}{\mu^2}\phi\right) + \left(\alpha F' + \frac{2m}{\mu^2}H\right)\delta$$

(2) $$\frac{\partial \phi}{\partial \tau} = \left(N - \frac{2H}{\mu}\right)\frac{W}{\alpha} - \left(\frac{m}{\mu}H + \kappa_z M\right)\frac{U}{\alpha} + I\frac{H}{\alpha}\left(\frac{\partial W}{\partial \mu} + \frac{W}{\mu} + \frac{m}{\mu}U + \kappa_z V\right)$$
$$+\tilde{\eta}\left(L\phi - \frac{2m}{\mu^2}\psi\right) + \tilde{\eta}'\left(\frac{\partial \phi}{\partial \mu} + \frac{\phi}{\mu} + \frac{m}{\mu}\psi\right) - N'\delta - N\frac{\partial \delta}{\partial \mu}$$

(3) $$\kappa_z\tilde{\rho}\frac{\partial Y}{\partial \tau} = \frac{\kappa_z\tilde{\rho}\tilde{T}'}{\alpha}W + \kappa_z\Lambda\left(LY + \frac{Y}{\mu^2}\right)$$
$$+I(\gamma - 1)\frac{\kappa_z\tilde{\rho}\tilde{T}}{\alpha}\left(\frac{\partial W}{\partial \mu} + \frac{W}{\mu} + \frac{m}{\mu}U + \kappa_z V\right)$$
$$+4(\gamma - 1)\frac{\tilde{\eta}}{\beta}\left[\left(\kappa_z N + \frac{m}{\mu}M'\right)\frac{\phi}{\mu} - M'(L\psi) + \left(\kappa_z N - \frac{m}{\mu}M'\right)\left(\frac{m}{\mu}\psi + \frac{\partial \phi}{\partial \mu}\right)\right]$$
$$-2(\gamma - 1)\frac{\kappa_z}{\beta}(M'^2 + N^2)\delta$$

(4) $$\frac{\kappa'\tilde{\rho}}{\alpha S^2}\frac{\partial W}{\partial \tau} = \left[\frac{m}{\mu}\left(\kappa_z H - \frac{m}{\mu}M\right) - \frac{M'}{\mu}\right]\psi - M(L\psi) - M'\frac{\partial \psi}{\partial \mu}$$
$$+\left[\frac{m}{\mu}\left(\frac{M}{\mu} - M'\right) + \kappa_z\left(N + \frac{H}{\mu}\right)\right]\phi + \left(\kappa_z H - \frac{m}{\mu}M\right)\frac{\partial \phi}{\partial \mu}$$
$$+\frac{\beta\kappa_z}{2}\left(\tilde{\rho}\frac{\partial Y}{\partial \mu} + T\frac{\partial \mathscr{R}}{\partial \mu} + Y\tilde{\rho}' + \mathscr{R}\tilde{T}'\right)$$
$$+\frac{\kappa_z\tilde{\rho}\Gamma}{\alpha S^2}\left[\left(1 + \frac{I}{3}\right)(LW) + \frac{I}{3}\left(\frac{m^2}{\mu^2} + \kappa_z^2\right)W - \left(2 + \frac{I}{3}\right)\frac{m}{\mu^2}U\right.$$
$$\left.+\frac{Im}{3\mu}\frac{\partial U}{\partial \mu} + \frac{I\kappa_z}{3}\frac{\partial V}{\partial \mu}\right]$$

(5) $$\frac{\kappa_z\tilde{\rho}}{\alpha S^2}\frac{\partial U}{\partial \tau} = \left(\frac{m}{\mu^2}M + \kappa_z N\right)\psi + \left[M\left(\frac{m^2}{\mu^2} + \kappa_z^2\right)\right]\phi$$
$$+\left(\frac{m}{\mu}M\right)\frac{\partial \psi}{\partial \mu} - \frac{\beta\kappa_z m}{2\mu}(\tilde{\rho}Y + \tilde{T}\mathscr{R})$$
$$+\frac{\kappa_z\tilde{\rho}\Gamma}{\alpha S^2}\left[LU - \frac{2m}{\mu^2}W - \frac{Im}{3\mu}\left(\frac{\partial W}{\partial \mu} + \frac{W}{\mu} + \frac{m}{\mu}U + \kappa_z V\right)\right]$$

(6) $$\frac{\kappa_z\tilde{\rho}}{\alpha S^2}\frac{\partial V}{\partial \tau} = \left(\kappa_z M' - \frac{m}{\mu^2}H\right)\psi - \left(\frac{m}{\mu}H\right)\frac{\partial \psi}{\partial \mu} - \left[H\left(\frac{m^2}{\mu^2} + \kappa_z^2\right)\right]\phi$$
$$-\frac{\beta\kappa_z^2}{2}(\tilde{\rho}Y + \tilde{T}\mathscr{R}) + \frac{\kappa_z\tilde{\rho}\Gamma}{\alpha S^2}\left[LV + \frac{V}{\mu^2} - \frac{I\kappa_z}{3}\left(\frac{\partial W}{\partial \mu} + \frac{W}{\mu} + \frac{m}{\mu}U + \kappa_z V\right)\right]$$

(7) $$\frac{\partial \mathscr{R}}{\partial \tau} = \frac{\tilde{\rho}'}{\alpha}W + I\frac{\tilde{\rho}}{\alpha}\left(\frac{\partial W}{\partial \mu} + \frac{W}{\mu} + \frac{m}{\mu}U + \kappa_z V\right)$$

(8) $$P = \tilde{\rho}Y + T\mathscr{R}$$

Using the dimensionless variables, the system of linearized hydromagnetic equations for the general case with compressibility, viscosity, and thermal conductivity is presented in Table 3.1. The parameter I in these dimensionless equations indicates those terms which would vanish if the fluid was assumed to be incompressible.

3.2. *Difference Equations*

In this section the finite difference equations for the hydromagnetic models are described. The equations are presented in Eulerian form in which the independent spatial variable refers to a fixed coordinate system through which the fluid moves. The flow is characterized by a time-dependent velocity field which is determined by solving an initial value problem.

In order to solve the systems of equations, the continuous space–time domain on which the equations hold is replaced by a discrete space–time mesh. For the space–time mesh to be used, the superscript n denotes the time level for the independent variable τ, and the subscript j denotes the spatial mesh point for the independent variable μ. We have

$$\begin{aligned} &\tau \geqslant 0, && \mu \geqslant 0, \\ &\tau^n = n\,\Delta\tau, && n = 0, 1, 2,..., \\ &\mu_j = j\,\Delta\mu, && j = 0, 1, 2,..., J, \\ &\mu_J = J\,\Delta\mu = \mu_W . \end{aligned} \tag{36}$$

It is assumed that values of all the dependent variables are known at all spatial mesh points at a time τ^n, and the problem is to determine their values at a later time τ^{n+1}. To solve the problem, the differential equations are approximated at each spatial point by finite difference equations which are algebraic in form and which relate the dependent variables at time τ^{n+1} to the dependent variables at time τ^n. To numerically solve a system of m differential equations in m dependent variables on a mesh consisting of J points, a set of $m \times J$ algebraic equations in $m \times J$ unknowns must be solved at time τ^{n+1}.

For the hydromagnetic models to be examined here, it is desired to find $\psi(\mu, \tau)$, $\phi(\mu, \tau)$, $T(\mu, \tau)$, $W(\mu, \tau)$, $U(\mu, \tau)$, $V(\mu, \tau)$, $\mathscr{R}(\mu, \tau)$, and $\delta(\mu, \tau)$ on the domain $0 \leqslant \mu \leqslant \mu_W$, and where the initial distributions of these functions are given. The notation for the dependent variables is such that $\psi_j{}^n = \psi(\mu_j, \tau^n)$, $\phi_j{}^n = \phi(\mu_j, \tau^n)$, $T_j{}^n = T(\mu_j, \tau^n)$, etc. It is assumed that the dependent variables and their derivatives are single-valued, finite and continuous functions of the independent variables μ and τ.

The operator L, as defined in Eq. (35), is given in finite-difference form as

$$(LX)_j^n = \frac{X_{j+1}^n - 2X_j{}^n + X_{j-1}^n}{(\Delta\mu)^2} + \frac{1}{\mu_j}\frac{X_{j+1}^n - X_{j-1}^n}{2\Delta\mu} - \left(\frac{m^2+1}{\mu_j{}^2} + \kappa_z{}^2\right) X_j{}^n, \tag{37}$$

$$\begin{aligned} (LX)_j^n = {} & X_{j+1}^n \left[\frac{1}{(\Delta\mu)^2} + \frac{1}{2\mu_j\,\Delta\mu}\right] \\ & - X_j{}^n \left[\frac{2}{(\Delta\mu)^2} + \frac{m^2+1}{\mu_j{}^2} + \kappa_z{}^2\right] + X_{j-1}^n \left[\frac{1}{(\Delta\mu)^2} - \frac{1}{2\mu_j\,\Delta\mu}\right]. \end{aligned} \tag{38}$$

The systems of hydromagnetic equations are differenced implicitly with a weighting factor l, where $0 \leqslant l \leqslant 1$. For $l = 0$, the differencing scheme becomes fully explicit, i.e., the finite-difference equations are forward differenced and are uncoupled in the unknowns, each equation giving one of the unknowns X_j^{n+1} directly in terms of the known quantities X_j^n. For $l = 1$, the differencing scheme becomes fully implicit, i.e., the finite-difference equations are backward differenced and are coupled in the unknowns, and a system of simultaneous equations must be solved to obtain X_j^{n+1}. For stability [6, 7], $\frac{1}{2} \leqslant l \leqslant 1$, and for all of the results to be discussed in this report, a value of $l = \frac{1}{2}$ will be used, i.e., the equations will be completely centered in space and time.

For the general case with compressibility, viscosity, and thermal conductivity (Table 3.1), the finite-difference equations for $\psi(\mu, \tau)$ and $\phi(\mu, \tau)$, i.e., $B_{r1}(r, t)$ and $B_{\theta 1}(r, t)$, are

$$\frac{\psi_j^{n+1} - \psi_j{}^n}{\Delta\tau} = \tilde{\eta}_j[l(L\psi)_j^{n+1} + (1 - l)(L\psi)_j^n] - \tilde{\eta}_j \frac{2m}{\mu_j{}^2}[l\phi_j^{n+1} + (1 - l)\,\phi_j{}^n]$$
$$- F_j[lW_j^{n+1} + (1 - l)\,W_j{}^n] + \left(\alpha F_j' + \frac{2m}{\mu_j{}^2} H_j\right)[l\delta_j^{n+1} + (1 - l)\,\delta_j{}^n], \tag{39}$$

$$\frac{\phi_j^{n+1} - \phi_j{}^n}{\Delta\tau} = \tilde{\eta}_j[l(L\phi)_j^{n+1} + (1 - l)(L\phi)_j^n] - \tilde{\eta}_j \frac{2m}{\mu_j{}^2}[l\psi_j^{n+1} + (1 - l)\,\psi_j{}^n]$$
$$+ l\tilde{\eta}_j'\left[\frac{\phi_{j+1}^{n+1} - \phi_{j-1}^{n+1}}{2\Delta\mu} + \frac{\phi_j^{n+1}}{\mu_j} + \frac{m}{\mu_j}\psi_j^{n+1}\right]$$
$$+ (1 - l)\,\tilde{\eta}_j'\left[\frac{\phi_{j+1}^n - \phi_{j-1}^n}{2\Delta\mu} + \frac{\phi_j{}^n}{\mu_j} + \frac{m}{\mu_j}\psi_j{}^n\right]$$
$$+ \frac{1}{\alpha}\left(N_j - \frac{H_j}{\mu_j}\right)[lW_j^{n+1} + (1 - l)\,W_j{}^n]$$
$$+ \frac{H_j}{2\alpha\,\Delta\mu}[l(W_{j+1}^{n+1} - W_{j-1}^{n+1}) + (1 - l)(W_{j+1}^n - W_{j-1}^n)]$$
$$- \frac{\kappa_z M_j}{\alpha}[lU_j^{n+1} + (1 - l)\,U_j{}^n] + \frac{\kappa_z H_j}{\alpha}[lV_j^{n+1} + (1 - l)\,V_j{}^n]$$
$$- \frac{N_j}{2\Delta\mu}[l(\delta_{j+1}^{n+1} - \delta_{j-1}^{n+1}) + (1 - l)(\delta_{j+1}^n - \delta_{j-1}^n)]$$
$$- N_j'[l\delta_j^{n+1} + (1 - l)\,\delta_j{}^n]. \tag{40}$$

Note: In Eq. (40) the parameter $I = 1$.

The finite-difference form of the energy equation is

$$\begin{aligned}
&\frac{\kappa_z\tilde{\rho}_j}{\Delta\tau}(Y_j^{n+1} - Y_j^n) \\
&\quad = \kappa_z\Lambda\left\{l\left[(LY)_j^{n+1} + \frac{Y_j^{n+1}}{\mu_j^2}\right] + (1-l)\left[(LY)_j^n + \frac{Y_j^n}{\mu_j^2}\right]\right\} \\
&\qquad + 4(\gamma-1)\frac{\tilde{\eta}_j}{\beta}\, l\left[-M_j'(L\psi)_j^{n+1} + \left(\kappa_z N_j + \frac{m}{\mu_j}M_j'\right)\frac{\phi_j^{n+1}}{\mu_j}\right. \\
&\qquad \left. + \left(\kappa_z N_j - \frac{m}{\mu_j}M_j'\right)\left(\frac{m}{\mu_j}\psi_j^{n+1} + \frac{\phi_{j+1}^{n+1} - \phi_{j-1}^{n+1}}{2\Delta\mu}\right)\right] \\
&\qquad + 4(\gamma-1)\frac{\tilde{\eta}_j}{\beta}(1-l)\left[-M_j'(L\psi)_j^n + \left(\kappa_z N_j + \frac{m}{\mu_j}M_j'\right)\frac{\phi_j^n}{\mu_j}\right. \\
&\qquad \left. + \left(\kappa_z N_j - \frac{m}{\mu_j}M_j'\right)\left(\frac{m}{\mu_j}\psi_j^n + \frac{\phi_{j+1}^n - \phi_{j-1}^n}{2\Delta\mu}\right)\right] \\
&\qquad + I(\gamma-1)\frac{\kappa_z\tilde{\rho}_j\tilde{T}_j}{\alpha}\left\{l\left[\frac{W_{j+1}^{n+1} - W_{j-1}^{n+1}}{2\Delta\mu} + \frac{W_j^{n+1}}{\mu_j} + \frac{m}{\mu_j}U_j^{n+1} + \kappa_z V_j^{n+1}\right]\right. \\
&\qquad \left. + (1-l)\left[\frac{W_{j+1}^n - W_{j-1}^n}{2\Delta\mu} + \frac{W_j^n}{\mu_j} + \frac{m}{\mu_j}U_j^n + \kappa_z V_j^n\right]\right\} \\
&\qquad + \frac{\kappa_z\tilde{\rho}_j\tilde{T}_j'}{\alpha}\left[lW_j^{n+1} + (1-l)\,W_j^n\right] \\
&\qquad - 2(\gamma-1)\frac{\kappa_z}{\beta}(M_j'^2 + N_j^2)[l\delta_j^{n+1} + (1-l)\,\delta_j^n]. \qquad (41)
\end{aligned}$$

The finite-difference equations for the r, θ, and z components of the equation of motion are, respectively,

$$\begin{aligned}
&\frac{\kappa_z\tilde{\rho}_j}{\alpha S^2\Delta\tau}(W_j^{n+1} - W_j^n) \\
&\quad = -M_j[l(L\psi)_j^{n+1} + (1-l)(L\psi)_j^n] \\
&\qquad - \frac{M_j'}{2\Delta\mu}[l(\psi_{j+1}^{n+1} - \psi_{j-1}^{n+1}) + (1-l)(\psi_{j+1}^n - \psi_{j-1}^n)] \\
&\qquad + \left[\frac{m}{\mu_j}\left(\kappa_z H_j - \frac{m}{\mu_j}M_j\right) - \frac{M_j'}{\mu_j}\right][l\psi_j^{n+1} + (1-l)\,\psi_j^n] \\
&\qquad + \frac{1}{2\Delta\mu}\left(\kappa_z H_j - \frac{m}{\mu_j}M_j\right)[l(\phi_{j+1}^{n+1} - \phi_{j-1}^{n+1}) + (1-l)(\phi_{j+1}^n - \phi_{j-1}^n)] \\
&\qquad + \left[\kappa_z\left(N_j + \frac{H_j}{\mu_j}\right) + \frac{m}{\mu_j}\left(\frac{M_j}{\mu_j} - M_j'\right)\right][l\phi_j^{n+1} + (1-l)\,\phi_j^n]
\end{aligned}$$

$$+\frac{\beta\kappa_z\tilde{\rho}_j}{4\Delta\mu}\left[l(Y_{j+1}^{n+1}-Y_{j-1}^{n+1})+(1-l)(Y_{j+1}^{n}-Y_{j-1}^{n})\right]$$

$$+\frac{\beta\kappa_z\tilde{\rho}_j'}{2}\left[lY_j^{n+1}+(1-l)\,Y_j^{n}\right]$$

$$+\frac{\kappa_z\tilde{\rho}_j\Gamma}{\alpha S^2}\left\{\left(1+\frac{I}{3}\right)\left[l(LW)_j^{n+1}+(1-l)(LW)_j^{n}\right]\right.$$

$$+\frac{I}{3}\left(\frac{m^2}{\mu_j{}^2}+\kappa_z{}^2\right)\left[lW_j^{n+1}+(1-l)\,W_j{}^{n}\right]$$

$$-\left(2+\frac{I}{3}\right)\frac{m}{\mu_j{}^2}\left[lU_j^{n+1}+(1-l)\,U_j{}^{n}\right]$$

$$+\frac{I}{6\Delta\mu}\frac{m}{\mu_j}\left[l(U_{j+1}^{n+1}-U_{j-1}^{n+1})+(1-l)(U_{j+1}^{n}-U_{j-1}^{n})\right]$$

$$\left.+\frac{I\kappa_z}{6\Delta\mu}\left[l(V_{j+1}^{n+1}-V_{j-1}^{n+1})+(1-l)(V_{j+1}^{n}-V_{j-1}^{n})\right]\right\}$$

$$+\frac{\beta\kappa_z\tilde{T}_j}{4\Delta\mu}\left[l(\mathscr{R}_{j+1}^{n+1}-\mathscr{R}_{j-1}^{n+1})+(1-l)(\mathscr{R}_{j+1}^{n}-\mathscr{R}_{j-1}^{n})\right]$$

$$+\frac{\beta\kappa_z\tilde{T}_j'}{2}\left[l\mathscr{R}_j^{n+1}+(1-l)\,\mathscr{R}_j{}^{n}\right], \tag{42}$$

$$\frac{\kappa_z\tilde{\rho}_j}{\chi S^2\,\Delta\tau}\left(U_j^{n+1}-U_j{}^{n}\right)$$

$$=\left(\frac{m}{\mu_j{}^2}M_j+\kappa_z N_j\right)\left[l\psi_j^{n+1}+(1-l)\,\psi_j{}^{n}\right]$$

$$+M_j\left(\frac{m^2}{\mu_j{}^2}+\kappa_z{}^2\right)\left[l\phi_j^{n+1}+(1-l)\,\phi_j{}^{n}\right]$$

$$+\frac{mM_j}{2\mu_j\,\Delta\mu}\left[l(\psi_{j+1}^{n+1}-\psi_{j-1}^{n+1})+(1-l)(\psi_{j+1}^{n}-\psi_{j-1}^{n})\right]$$

$$-\frac{\beta\kappa_z m}{2\mu_j}\left[l(\tilde{\rho}_jY_j^{n+1}+\tilde{T}_j\mathscr{R}_j^{n+1})+(1-l)(\tilde{\rho}_jY_j{}^{n}+\tilde{T}_j\mathscr{R}_j{}^{n})\right]$$

$$+\frac{\kappa_z\tilde{\rho}_j\Gamma}{\alpha S^2}\left\{l(LU)_j^{n+1}+(1-l)(LU)_j^{n}-2\frac{m}{\mu_j{}^2}\left[lW_j^{n+1}+(1-l)\,W_j{}^{n}\right]\right.$$

$$-\frac{Im}{6\mu_j\,\Delta\mu}\left[l(W_{j+1}^{n+1}-W_{j-1}^{n+1})+(1-l)(W_{j+1}^{n}-W_{j-1}^{n})\right]$$

$$-\frac{Im}{3\mu_j}\left[l\left(\frac{W_j^{n+1}}{\mu_j}+\frac{m}{\mu_j}\,U_j^{n+1}+\kappa_z V_j^{n+1}\right)\right.$$

$$\left.\left.+(1-l)\left(\frac{W_j{}^{n}}{\mu_j}+\frac{m}{\mu_j}\,U_j{}^{n}+\kappa_z V_j{}^{n}\right)\right]\right\}, \tag{43}$$

$$\frac{\kappa_z\tilde{\rho}_j}{\alpha S^2\,\Delta\tau}(V_j^{n+1}-V_j^n)$$

$$=\left(\kappa_z M_j'-\frac{m}{\mu_j^2}H_j\right)[l\psi_j^{n+1}+(1-l)\,\psi_j^n]$$

$$-\frac{mH_j}{2\mu_j\,\Delta\mu}[l(\psi_{j+1}^{n+1}-\psi_{j-1}^{n+1})+(1-l)(\psi_{j+1}^n-\psi_{j-1}^n)]$$

$$-H_j\left(\frac{m^2}{\mu_j^2}+\kappa_z^2\right)[l\phi_j^{n+1}+(1-l)\,\phi_j^n]$$

$$+\frac{\kappa_z\tilde{\rho}_j\Gamma}{\alpha S^2}\left\{l(LV)_j^{n+1}+(1-l)(LV)_j^n+\frac{1}{\mu_j^2}[lV_j^{n+1}+(1-l)V_j^n]\right.$$

$$-\frac{I\kappa_z}{6\Delta\mu}[l(W_{j+1}^{n+1}-W_{j-1}^{n+1})+(1-l)(W_{j+1}^n-W_{j-1}^n)]$$

$$-\frac{I\kappa_z}{3}\left[l\left(\frac{W_j^{n+1}}{\mu_j}+\frac{m}{\mu_j}U_j^{n+1}+\kappa_z V_j^{n+1}\right)\right.$$

$$\left.\left.+(1-l)\left(\frac{W_j^n}{\mu_j}+\frac{m}{\mu_j}U_j^n+\kappa_z V_j^n\right)\right]\right\}. \tag{44}$$

Finally, the finite-difference approximations to the continuity equation and the equation of state are

$$\frac{\mathscr{R}_j^{n+1}-\mathscr{R}_j^n}{\Delta\tau}=\frac{I\tilde{\rho}_j}{2\alpha\,\Delta\mu}[l(W_{j+1}^{n+1}-W_{j-1}^{n+1})+(1-l)(W_{j+1}^n-W_{j-1}^n)]$$

$$+\frac{1}{\alpha}\left(I\frac{\tilde{\rho}_j}{\mu_j}+\rho_j'\right)[lW_j^{n+1}+(1-l)\,W_j^n]$$

$$+\frac{Im\tilde{\rho}_j}{\alpha\mu_j}[lU_j^{n+1}+(1-l)\,U_j^n]$$

$$+\frac{I\kappa_z\tilde{\rho}_j}{\alpha}[lV_j^{n+1}+(1-l)\,V_j^n], \tag{45}$$

$$lP_j^{n+1}+(1-l)\,P_j^n=\tilde{\rho}_j[lY_j^{n+1}+(1-l)\,Y_j^n]+\tilde{T}_j[l\mathscr{R}_j^{n+1}+(1-l)\,\mathscr{R}_j^n]. \tag{46}$$

3.3. *Method of Solution*

It is desired to solve the initial-value problem described by the systems of component equations as given in Table 3.1. Equations (39)–(44) are written as a single vector difference equation as follows:

$$-A_j\overline{U}_{j+1}^{n+1}+B_j\overline{U}_j^{n+1}-C_j\overline{U}_{j-1}^{n+1}=d_j^n \qquad \text{for } j=0,1,\ldots,J. \tag{47}$$

Here we use the superscript n to denote time levels, and the subscript j to denote mesh points in r. The vector $\bar{U}$ is defined as

$$\bar{U} = \begin{bmatrix} B_{r1} \\ B_{\theta 1} \\ T_1 \\ v_{r1} \\ v_{\theta 1} \\ v_{z1} \end{bmatrix} \sim \begin{bmatrix} \psi \\ \phi \\ \Upsilon \\ W \\ U \\ V \end{bmatrix} \tag{48}$$

and A, B, and C are 6×6 matrices. The matrix elements A, B, C, and d are given in detail elsewhere [8]. The system is linear, that is the A, B, and C depend only on r through the zero-order functions and their derivatives; consequently, we can use the familiar algorithm for linear tridiagonal systems, i.e., let

$$\bar{U}_j^{n+1} = E_j \bar{U}_{j+1}^{n+1} + F_j^n \tag{49}$$

where the E_j , F_j^n are determined from the recurrence relations

$$\begin{aligned} E_j &= (B_j - C_j E_{j-1})^{-1} A_j , \\ F_j^n &= (B_j - C_j E_{j-1})^{-1} (d_j^n + C_j F_{j-1}^n). \end{aligned} \tag{50}$$

The above calculation involves inverting a 6×6 matrix at each mesh point, which is done numerically.

Equation (12) for the variable $\rho_1(r, t)$ is not a diffusion equation so we solve it simultaneously, but with a separate difference equation (45).

The perturbed resistivity $\eta_1(r, t)$ is computed from ρ_1 , T_1 , and $\mathbf{B}_1$ using a standard resistivity expression, i.e., we have

$$\begin{aligned} \eta_0(r) &= F(\rho_0 , T_0 , \mathbf{B}_0), \\ \eta(r, t) &= F(\rho_0 + \rho_1 , T_0 + T_1 , \mathbf{B}_0 + \mathbf{B}_1), \\ \eta_1(r, t) &= \eta(r, t) - \eta_0(r), \end{aligned}$$

where F is a given function.

3.4. *Boundary and Initial Conditions*

The required boundary conditions were described in Eqs. (16)–(22). The boundary conditions at $r = 0$ are used to find the E_0 and F_0^n matrices of the tridiagonal algorithm (49), and the boundary conditions at $r = R_W$ are used to determine U_J^n. Differencing Eqs. (16)–(22), using the points $j = 0$ and $j = 1$, and then using (49), the boundary conditions and the matrices E_0 and F_0^n for all t for $r = 0$ are:

$\underline{m = 0}$

$$(B_{r1})_0 = (B_{\theta 1})_0 = (v_{r1})_0 = (v_{\theta 1})_0 = 0,$$

$$(T_1)_0 = (T_1)_1 ,$$

$$(v_{z1})_0 = (v_{z1})_1 ,$$

$$(\rho_1)_0 = (\rho_1)_1 ,$$

$$E_0 = \begin{bmatrix} 0 & & & & & 0 \\ & 0 & & & & \\ & & 1 & & & \\ & & & 0 & & \\ & & & & 0 & \\ 0 & & & & & 1 \end{bmatrix},$$

$$F_0^n = 0, \qquad \text{the null vector,}$$

$\underline{m = 1}$

$$(B_{r1})_0 = (B_{r1})_1 ,$$

$$(B_{\theta 1})_0 = (B_{\theta 1})_1 ,$$

$$(T_1)_0 = 0,$$

$$(v_{r1})_0 = (v_{r1})_1 ,$$

$$(v_{\theta 1})_0 = (v_{\theta 1})_1 ,$$

$$(v_{z1})_0 = 0,$$

$$(\rho_1)_0 = 0,$$

$$E_0 = \begin{bmatrix} 1 & & & & & 0 \\ & 1 & & & & \\ & & 0 & & & \\ & & & 1 & & \\ & & & & 1 & \\ 0 & & & & & 0 \end{bmatrix}$$

$$F_0^n = 0, \qquad \text{the null vector}$$

$\underline{m \geqslant 2}$

$$(B_{r1})_0 = (B_{\theta 1})_0 = (T_1)_0 = (v_{r1})_0 = (v_{\theta 1})_0 = (v_{z1})_0 = (\rho_1)_0 = 0,$$

$$E_0 = 0, \qquad \text{the null matrix,}$$

$$F_0^n = 0, \qquad \text{the null vector.}$$

At the outer wall R_W where $j = J$, the boundary conditions specified in Eqs. (19)–(22) can be expressed in finite-difference form as

$$(B_{r1})_J^n = (v_{r1})_J^n = (T_1)_J^n = (\rho_1)_J^n = 0, \tag{51}$$

$$(B_{\theta 1})_J^{n+1} = \frac{-imR_W}{m^2 + k_z{}^2 R_W{}^2} \frac{(B_{r1})_{J-1}^n}{\Delta r}, \tag{52}$$

$$(v_{\theta 1})_J^{n+1} = \frac{-imR_W}{m^2 + k_z{}^2 R_W{}^2} \frac{(v_{ri})_{J-1}^n}{\Delta r}, \tag{53}$$

$$(v_{z1})_J^{n+1} = \frac{-ik_z R_W{}^2}{m^2 + k_z{}^2 R_W{}^2} \frac{(v_{r1})_{J-1}^n}{\Delta r}, \tag{54}$$

where an explicit differencing has been used by approximating B_{r1} and v_{r1} at the previous time step, and where use has been made of (51).

For the special case of $m = 0$, the boundary conditions at R_W reduce to

$$(B_{r1})_J^n = (B_{\theta 1})_J^n = (T_1)_J^n = (v_{r1})_J^n = (v_{\theta 1})_J^n = (\rho_1)_J^n = 0, \tag{55}$$

$$(v_{z1})_J^{n+1} = -\frac{i}{k_z \Delta r} (v_{r1})_{J-1}^n . \tag{56}$$

In order to begin the calculation, an initial perturbation must be applied to one of the dependent variables, usually $v_{r1}(r, 0)$. If the method of solving the linearized systems of hydromagnetic equations is consistent with the original assumptions, then the results should be independent of this initial perturbation. A variety of forms for this initial perturbation were tested; for example

$$v_{r1}(r, 0) = -(r - r_0)\, e^{-C_0 |r - r_0|}, \tag{57}$$

where r_0 is an adjustable constant which determines the zero point of the initial profile, and C_0 is an adjustable constant which is used to vary the shape of the initial profile. Using (57) various $v_{r1}(r, 0)$ profiles were tested using values of $C_0 = 1, 2, 5, 10, 20$ in combination with $r_0 = R_W$, $R_W/2$, $R_W/3$, $R_W/4$. For all combinations of C_0 and r_0, it was found that the results were independent of the initial perturbation for both $m = 0$ and $m \geqslant 1$.

Other analytic forms for the initial perturbation were also tested, in particular,

$$v_{r1}(r, 0) = e^{-C_0} \left[1 - \left(\frac{r}{R_W}\right)^2\right] \qquad \text{for} \quad m = 1, \tag{58}$$

$$v_{r1}(r, 0) = e^{-C_0} \left(\frac{r}{R_W}\right)\left[1 - \left(\frac{r}{R_W}\right)^2\right] \qquad \text{for} \quad m \neq 1, \tag{59}$$

where here C_0 is an adjustable constant used to vary the magnitude of the perturbation and where the shapes of the profiles are independent of C_0. For values of C_0 ranging

from $C_0 = 1$ to $C_0 = 100$, the magnitude of the perturbation varies from approximately 10^{-1} to 10^{-44}, and for this range of values it was again found that the resultant profiles and growth rates were independent of the initial perturbation.

In general it was found that a form of initial perturbation profile as given by Eqs. (58) and (59) seemed to get the calculations started more smoothly at early time steps, and this form of perturbation is used for most of the equilibrium models discussed in this report. Since the magnitudes of the perturbed profiles grow with time, a value of $C_0 \approx 75$ was used so that for even the largest growth rates encountered, the problem settled down to an exponential growth long before the absolute magnitude of the profiles exceeded the limits of the computer.

3.5. *Computational Procedure*

In order to solve for the perturbed or first-order variables, the equilibrium or zero-order variables must be specified as functions of the radius. For the general case, the functions which must be specified are

$$\left(\frac{B_{\theta 0}}{B}\right), \quad \left(\frac{B_{z0}}{B}\right), \quad \left(\frac{T_0}{\langle T\rangle}\right), \quad \left(\frac{\rho_0}{\langle \rho_0\rangle}\right), \quad \left(\frac{\eta_0}{\langle \eta\rangle}\right),$$

on the domain $0 \leqslant r \leqslant R_W$. These functions then characterize the equilibrium model. To set up a particular problem for the general case, it is also necessary to specify the parameters

$$a, \quad m, \quad k_z, \quad \gamma, \quad n_i, \quad T_i, \quad B.$$

With the above quantities, the computer code then prepares the input needed to solve the systems of hydromagnetic equations.

The equilibrium functions and their derivatives are specified in analytic form and computed within the code. The exponential growth rate p is then computed using

$$p = (\partial\psi/\partial\tau)/\psi, \tag{60}$$

or in finite-difference form,

$$p_j^{n+1} = \frac{\psi_j^{n+1} - \psi_j^{n-1}}{2\psi_j{}^n\, \Delta\tau} \tag{61}$$

4. Applications

To begin the numerical study of resistive tearing instabilities in diffuse pinch geometries, an equilibrium magnetic field model is chosen which has a nontrivial analytic solution [9] and which also contains characteristics of actual pinch fields, namely diffuse currents and a reversed B_z. The model is referred to as the Lundquist [10] fields or the Bessel function model (BFM), and its analytic solution is compared with the numerical results in order to test the applicability of the linearized hydromagnetic equations and their associated computational solution.

The Bessel function model is a cylindrical force-free hydromagnetic equilibrium model with

$$\begin{aligned} B_{r0} &= 0, \\ B_{\theta 0} &= B_0 J_1(\nu r), \\ B_{z0} &= B_0 J_0(\nu r), \end{aligned} \tag{62}$$

where J_0 and J_1 are Bessel functions of the first kind, and B_0 and ν are constants. The force-free feature of the model is characterized by the vanishing of the Lorentz force, i.e., at equilibrium

$$(\nabla \times \mathbf{B}) \times \mathbf{B} = 0, \tag{63}$$

and this condition is satisfied by the Bessel function model as given in Eq. (62). The magnetic fields of a force-free configuration can also be expressed by

$$\nabla \times \mathbf{B} = \nu \mathbf{B}, \tag{64}$$

where ν is in general a scalar function of space satisfying

$$\mathbf{B} \cdot \nabla \nu = 0, \tag{65}$$

and Eqs. (64) and (65) are satisfied by the BFM of (62) with $\nu =$ constant. The equilibrium profiles for the BFM with $\nu = 1$ are shown in Fig. 3, where it can be seen that the first two zeroes of B_{z0} (i.e., J_0) are $J_{0,1} = 2.405$ and $J_{0,2} = 5.520$, and the first zero of $B_{\theta 0}$ (i.e., J_1) is $J_{1,1} = 3.832$. The conducting plasma boundary R_w is placed at various radii, but in order to keep the equilibrium fields realistic, only one reversal in B_{z0} is considered, and this implies $R_w < 5.52$.

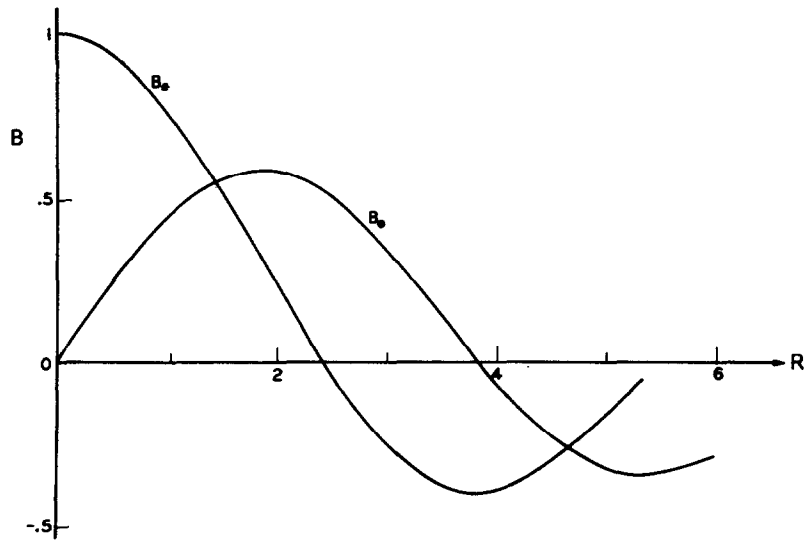

FIG. 3. Magnetic field profiles for the Bessel function model (BFM).

Using the force-free Bessel function model for the equilibrium magnetic fields, the regimes of stability/instability as predicted by analytic theory are compared with the computational results. Growth rates are calculated for various (m, k_z) modes and the results are presented in the form of stability diagrams [8]. Additional parametric studies are also performed to determine the specific dependence of the growth rates on the position of outer conducting wall R_W, on the axial wave number k_z, and on the magnetic Reynolds number S.

A small perturbation of the form given in Eqs. (58) and (59) with $C_0 = 75$ is applied

[redacted]

p becomes constant, i.e., until the growth becomes exponential. For a growing mode the perturbed variables increase with time, and for an exponential growth, p becomes a positive constant. For a stable mode the perturbed variables decay with time, and for an exponential decay, p becomes a negative constant. For some stable cases it was observed that the perturbed variables oscillate about the equilibrium values, never attaining an exponential growth or exponential decay. A mesh size of 101 points is used for all the problems to be discussed, and for a point at the center of the mesh, the time dependence of the perturbed radial magnetic field is shown in Fig. 4 for a

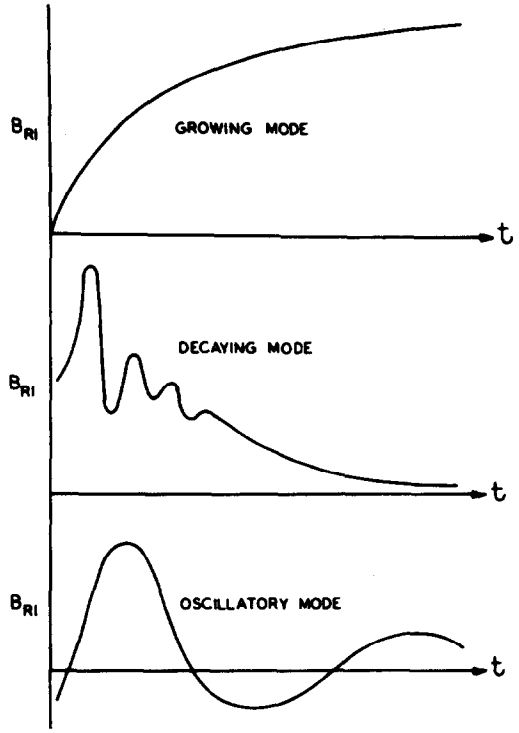

FIG. 4. Radial magnetic field behavior for a growing mode, a decaying mode, and an oscillatory mode.

typical growing mode, decaying mode, and oscillatory mode. The magnitudes of the three profiles have been arbitrarily scaled to fit the same plot. It can be seen in Fig. 4 that for the mesh point shown, the growing mode and the decaying mode settle down to an exponential growth and exponential decay, respectively. All other points on the mesh also settle down to an exponential growth or decay, but may do so at slightly earlier or later times than the point shown.

For an arbitrarily chosen set of parameters, the growth of a typical perturbation profile ψ is shown in Fig. 5. Except for the first few time steps, the perturbation retains

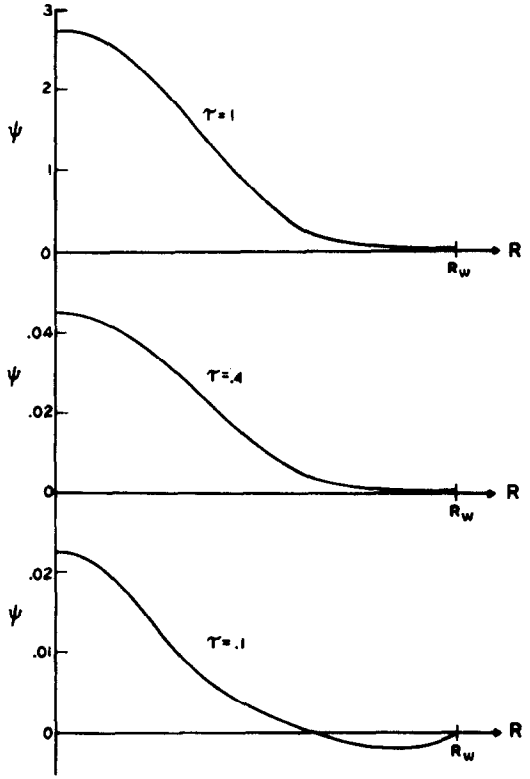

Fig. 5. Radial magnetic field profiles for $m = 1$, $R_w = 5$, $k_z = 0.3$, $S = 100$.

its shape as it grows. For the same problem, the behavior of the growth rate p with time is shown in Fig. 6, and it can be seen that after some initial fluctuation, the growth rate becomes constant. Since the linearized hydromagnetic model excludes all nonlinear effects, the growth rate will not saturate and the perturbed vairables will continue to grow (or decay) at an exponential rate for as long as the calculation is continued.

In order to determine realistic values for the equilibrium functions and the dissipative coefficients, characteristic values are chosen for the plasma number density n_i,

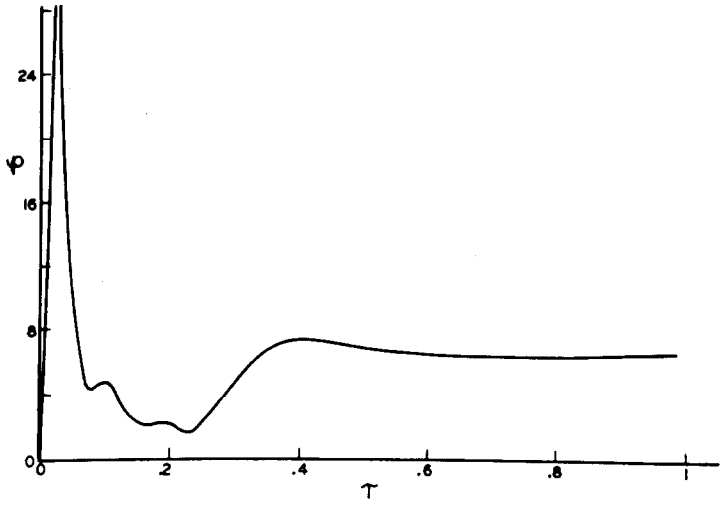

FIG. 6. Variation of the growth rate p with time for $m = 1$, $R_w = 5$, $k_z = .3$, $S = 100$.

TABLE 4.1

Characteristic Plasma Parameters

Resistivity	$\eta = 1.435 \times 10^{-8} \dfrac{\ln \lambda_c}{T_i^{3/2}}$ statohm-cm
Coulomb logarithm collision parameter	$\lambda_c = 1.239 \times 10^{4} \dfrac{T_i^{3/2}}{n_i^{1/2}}$
Viscosity	$\Gamma = 1.576 \times 10^{-14} \dfrac{n_i T_i}{B^2}$
Thermal conductivity	$\Lambda = 1.051 \times 10^{-13}(\gamma - 1) \dfrac{n_i T_i}{B^2}$
Plasma beta	$\beta_i = 3.469 \times 10^{-15} \dfrac{n_i T_i}{B^2}$
Magnetic Reynolds number	$S = 0.2122 \dfrac{aBT_i^{3/2}}{n_i^{1/2} \ln \lambda_c}$
Equilibrium temperature profile	$\hat{T}(\mu) = 1$
Equilibrium density profile	$\hat{\rho}(\mu) = 1$
Equilibrium resistivity profile	$\eta(\mu) = 1$

n_i = #/cm^3, T_i = °K, B = gauss, a = cm

temperature T_i, and magnetic field B. These characteristic values are then used in standard relations to get characteristic values for the resistivity, viscosity, and thermal conductivity. The appropriate characteristic values are then combined to determine the normalization for the dimensionless viscosity Γ, the dimensionless thermal conductivity Λ, the magnetic Reynolds number S, and the dimensionless parameter β. The characteristic values and dimensionless plasma parameters which are used in this report are summarized in Table 4.1.

Using the FFBFM with the computer code for the general case, it was found that the instabilities occurred generally in the same region of (k_z, R_w) space as was found for the incompressible case [8, 9], and the same general type of dependence of the growth rate on k_z and R_w was observed. Some typical results for the $m = 0$ and $m = 1$ modes are shown in Fig. 7. It is possible to obtain growth rates for the $m = 0$ mode

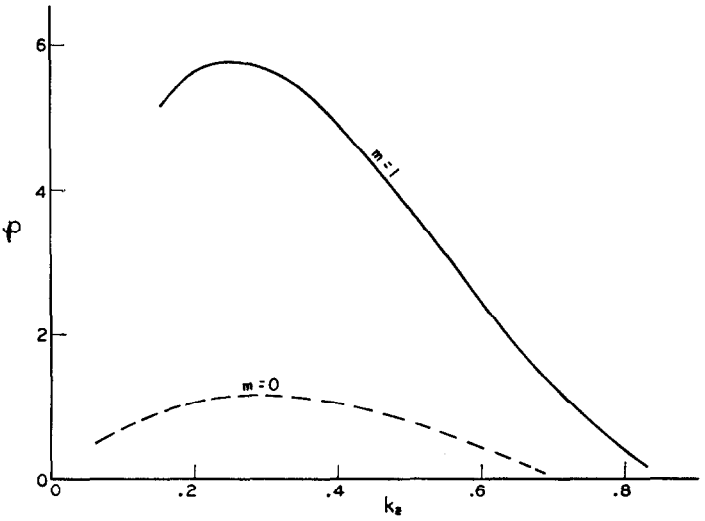

FIG. 7. Variation of the growth rate p with k_z for the BFM for the general case with $m = 0$, 1, $R_w = 5.5$, $n = 10^{15}/\text{cm}^3$, $T = 16.7$ eV, $B = 1950$ gauss.

in which viscosity is neglected, and Fig. 8 compares these growth rates with those of the viscous case. As might be expected, the addition of viscosity slows down the growth rate and in addition the most unstable wave number shifts to a slightly lower value for the viscous case.

For a given ratio of (n/B^2), S varies with $T^{3/2}$, and the variation of the growth rate p with S corresponds to the effect of increasing T or β in the general case. For $n = 10^{15}/\text{cm}^3$ and $B = 1950$ gauss, β is in the range $0.1 \lesssim \beta \lesssim 1$ for $0.01 \lesssim T$ (keV) $\lesssim 0.1$, and the corresponding values for S are in the range $50 \lesssim S \lesssim 1200$. Some representative values are given in Fig. 9 for the $m = 0$ and $m = 1$ modes.

For the $m = 1$ mode at $k_z = 0.4$, the profiles of the perturbed variables B_{r1}, $B_{\theta 1}$, v_{r1}, $v_{\theta 1}$, v_{z1}, T_1, η_1, ρ_1, and p_1 are shown in Figs. 10a–h.

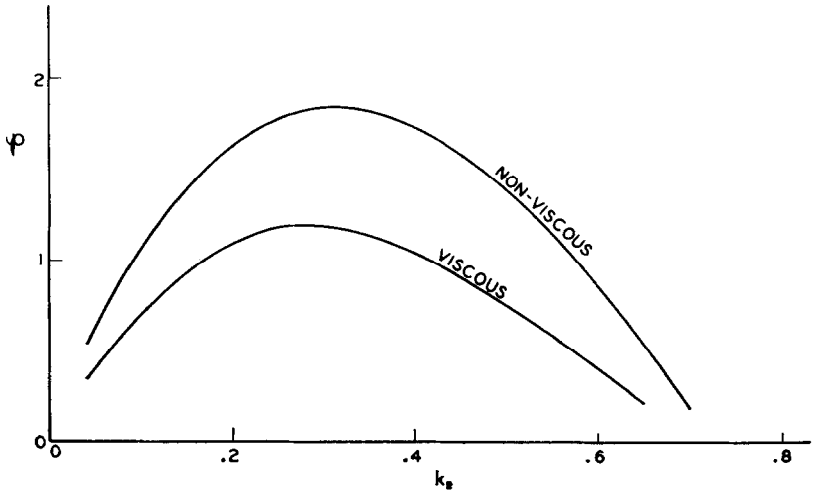

FIG. 8. Comparison between growth rates for viscous and nonviscous cases for the BFM for $m = 0$, $R_w = 5.5$, $n = 10^{15}/\text{cm}^3$, $T = 16.7$ eV, $B = 1950$ gauss.

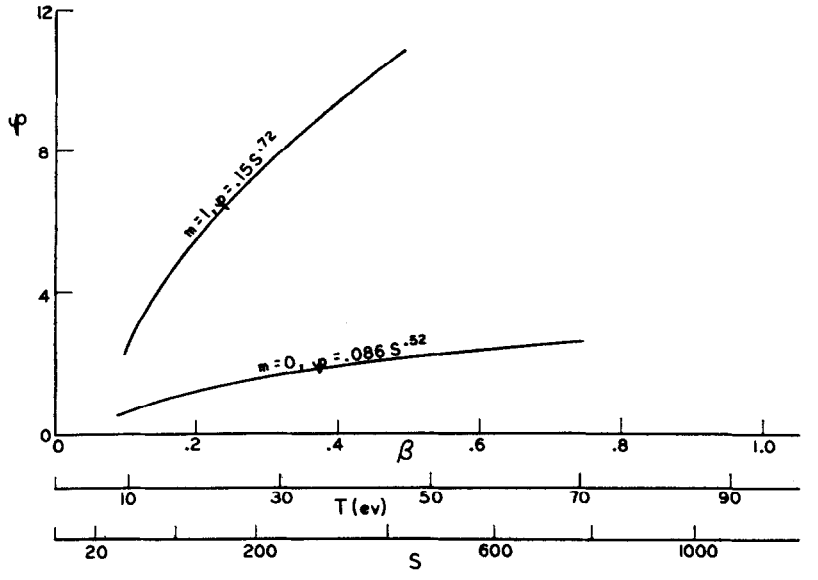

FIG. 9. Variation of the growth rate p with S, T, and β for the general case with $m = 0$, 1, $R_w = 5.5$, $k_z = 0.4$, $n = 10^{15}/\text{cm}^3$, $B = 1950$ gauss.

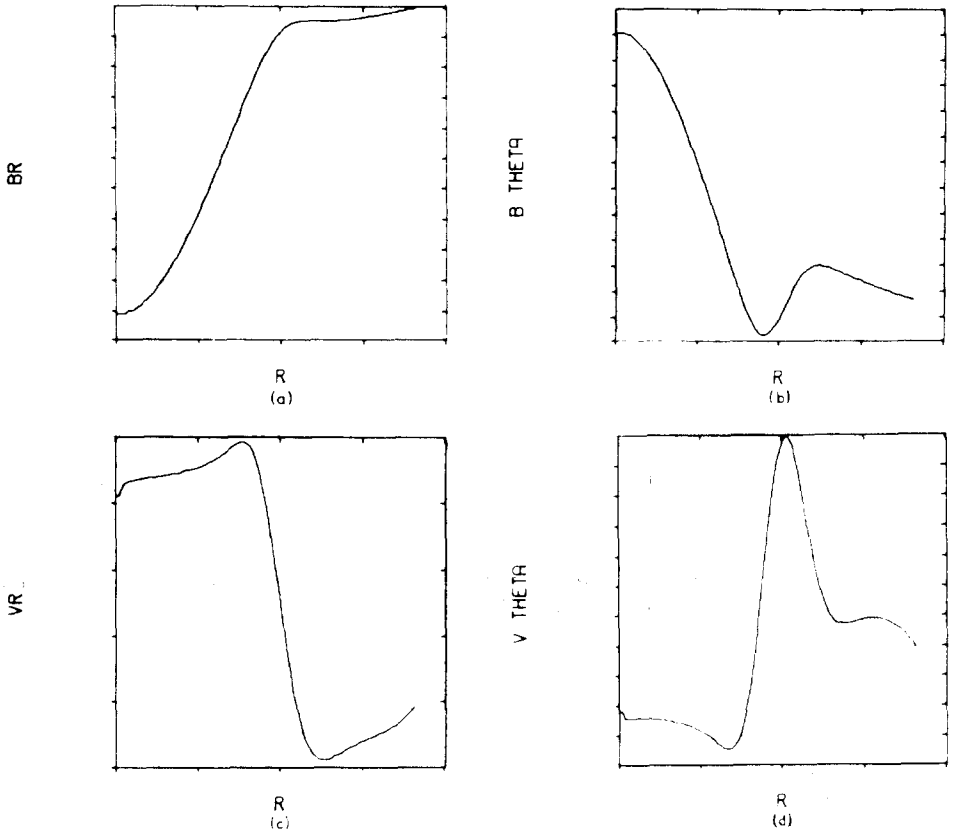

FIG. 10. Perturbed profiles for the BFM for the general case with $m = 1$, $R_w = 5.5$, $k_z = .4$, $n = 10^{15}/\text{cm}^3$, $T = 16.7$ eV, $B = 1950$ gauss.

In summary, it is found that the computer model can be used to examine resistive tearing instabilities for reversed field pinch configurations, and that the computed growth rates for the special case of the force-free Bessel function model occur in the regions of (k_z, R_w) space predicted by analytic theory. The inclusion of finite resistivity in the analysis of the FFBFM yields the result that the conducting wall must be placed approximately 2% closer to the plasma in order to ensure stability against resistive tearing modes as well as ideal MHD modes. Since the BFM as used here is a force-free equilibrium, there are no pressure gradients as usually exist in real plasmas, so a more realistic reversed field pinch model which contains a pressure gradient will now be discussed.

For high-beta plasmas, Robinson [11] used the hydromagnetic energy principle to examine the MHD stability of diffuse pinch configurations for infinitely con-

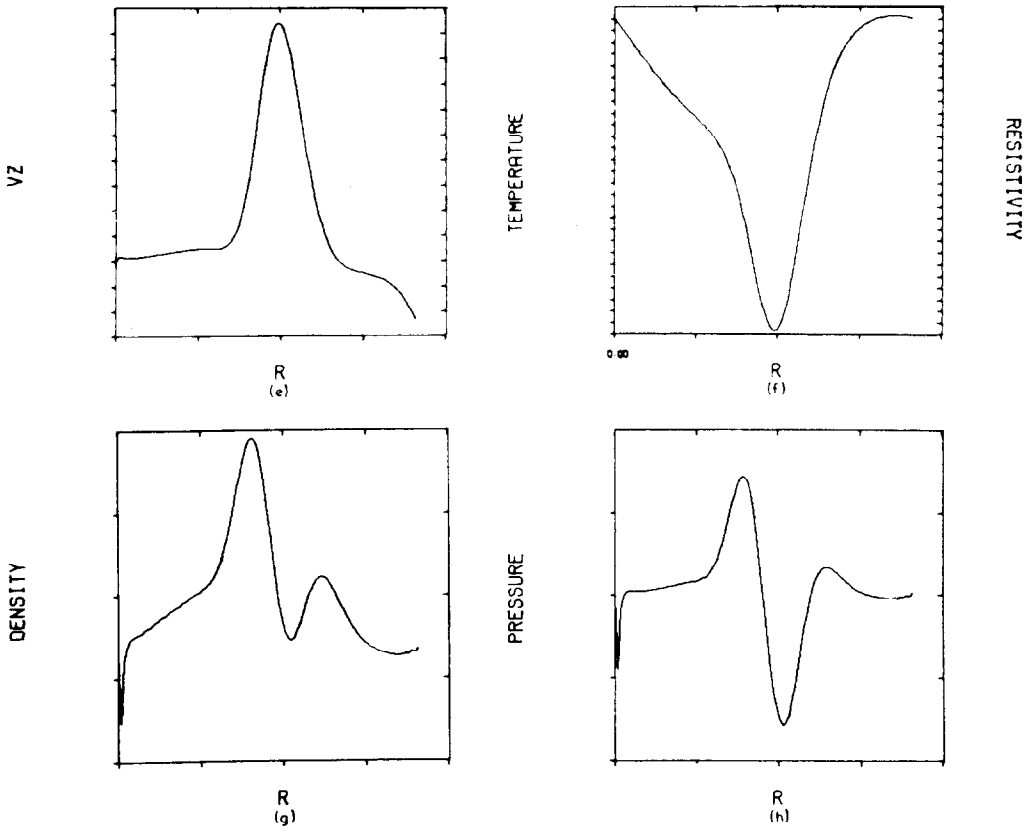

FIGURE 10 (*continued*).

ducting plasmas surrounded by perfectly conducting walls. He constructed a reversed field configuration which has $\beta \sim 31\,\%$. This configuration will be referred to as the pitch and pressure model (PPM). For the PPM, a variety of parametric studies [8, 12] are performed to determine the specific dependence of the growth rates on the azimuthal wave number m, the axial wave number k_z, the position of the outer conducting wall R_w, the magnetic Reynolds number S, and the value of β. In Fig. 11 is the reversed field pinch equilibrium given by the PPM, and in Fig. 12 we show the variation of the growth rate p. The inclusion of finite resistivity in the analysis of the PPM indicates that for positive k_z values the conducting wall must be placed approximately 22 % closer to the plasma in order to ensure stability against resistive tearing modes as well as ideal MHD modes, and up to 50 % closer to ensure stability for negative k_z values.

The code has also been used for studies of instabilities in the High-Beta Toroidal Experiment [13–15] at the Culham Laboratory, U.K.

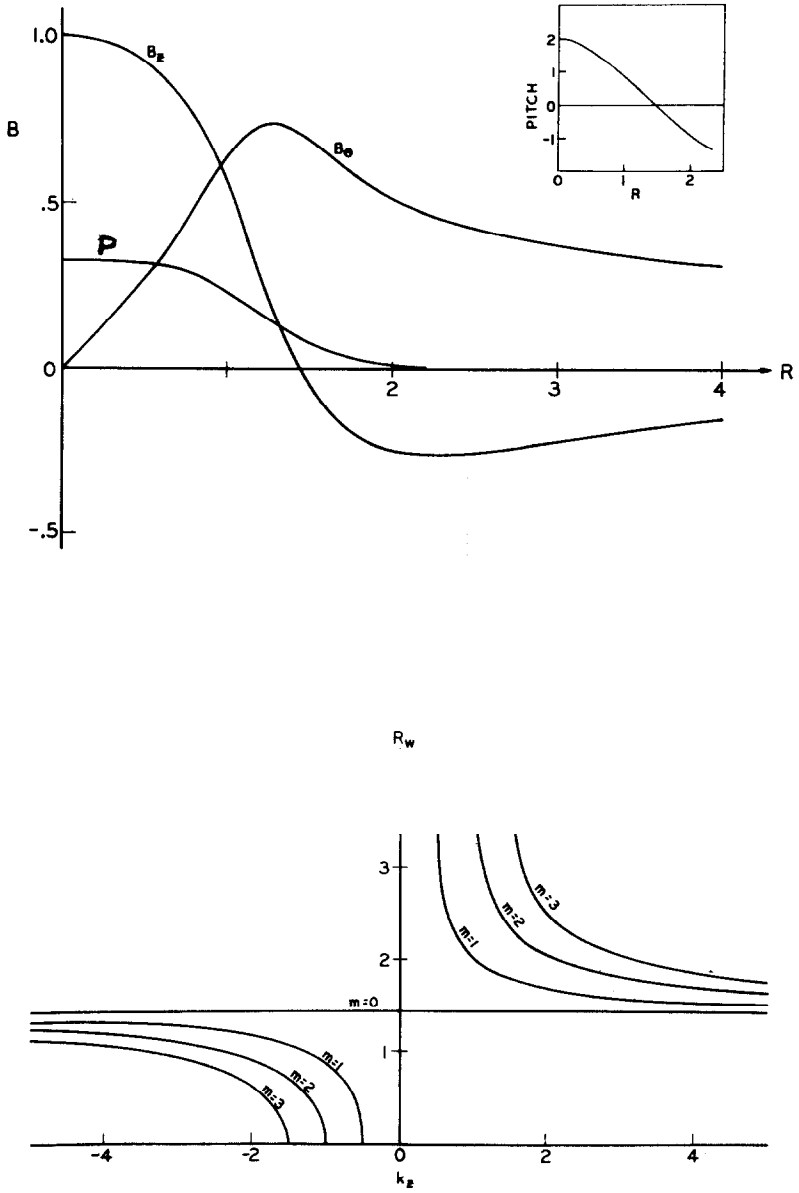

FIG. 11. (a) B_θ, B_z, pressure and pitch profiles for the Pitch and Pressure model (PPM). (b) $F = \vec{k} \cdot \vec{B} = 0$ curves for the PPM.

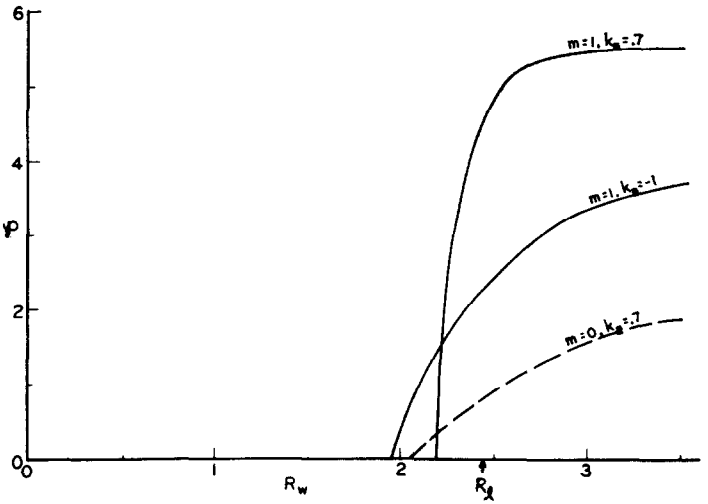

FIG. 12. Variation of the growth rate p with R_w for the PPM for the general case with $n = 1.7 \times 10^{15}/\text{cm}^3$, $T = 18.5$ eV, $B = 2000$ gauss. The maximum wall position for complete MHD stability is denoted by R_t.

REFERENCES

1. H. P. FURTH, J. KILLEEN, AND M. N. ROSENBLUTH, *Phys. Fluids* **6** (1963), 459.
2. B. COPPI, J. M. GREENE, AND J. L. JOHNSON, *Nucl. Fusion* **6** (1966), 101.
3. J. KILLEEN, Computational problems plasma physics and controlled thermonuclear research, *in* "Physics of Hot Plasmas" (B. J. Rye and J. C. Taylor, Eds.), p. 202, Plenum, New York, 1970.
4. J. E. CROW, J. KILLEEN, AND D. C. ROBINSON, Sixth European Conference on Controlled Fusion and Plasma Physics, Moscow, p. 269, (1973).
5. D. C. ROBINSON, UKAEA Culham Laboratory, Abingdon, Berkshire, England, private communication, 1973.
6. R. D. RICHTMYER AND K. W. MORTON, "Difference Methods for Initial Value Problems," 2nd ed., Interscience, New York, 1967.
7. J. KILLEEN, Computational problems in magnetohydrodynamics, *in* "Information Processing 71," pp. 1191–1205, North-Holland, Amsterdam, 1972.
8. J. A. DIBIASE, "Numerical Studies of Resistive Instabilities in Diffuse Pinches," Ph.D. Thesis, University of California, Davis, Lawrence Livermore Laboratory Report UCRL-51591, 1974.
9. R. D. GIBSON AND K. J. WHITEMAN, *Plasma Phys.* **10** (1968), 1101.
10. S. LUNDQUIST, *Phys. Rev.* **83** (1951), 307.
11. D. C. ROBINSON, *Plasma Phys.* **13** (1971), 439.
12. J. A. DIBIASE, J. KILLEEN, D. C. ROBINSON, AND D. SCHNACK, *in* "Third Topical Conference on Pulsed High Beta Plasmas, Culham (1975," pp. 283–289, Paper B1-9, Pergamon, Oxford, 1976.
13. E. P. BUTT *et al.*, *in* "Plasma Physics and Controlled Nuclear Fusion Research 1974," Vol. 3, p. 417, Proceedings of the Tokyo Conference, IAEA, Vienna 1975.
14. C. W. GOWERS *et al.*, *in* "Sixth Conference on Plasma Physics and Controlled Nuclear Fusion Research, Berchtesgaden 1976," IAEA Vienna, paper CN35-E-2.
15. A. J. L. VERHAGE, A. S. FURZER, AND D. C. ROBINSON, "Observations of Large Amplitude Helical Kink Instabilities and Field Reversal in a Fast Pinch Experiment," CLM-P 463, submitted to *Nuclear Fusion*.